ACTA ACUSTICA UNITED WITH ACUSTICA
Vol. 99 (2013) 694 – 702
DOI 10.3813/AAA.918648

# On the Acoustic Transfer Function of Slowly Tapered Small Horns Filled With Thermo-Viscous Fluid

Petr Honzík, Stéphane Durand, Nicolas Joly, Michel Bruneau
LUNAM Université, LAUM (Laboratoire d'Acoustique de l'Université du Maine), UMR CNRS 6613, Avenue Olivier Messiaen, 72085 Le Mans, France. Petr.Honzik@gmail.com

**Summary**
When designing small scale acoustic devices, slowly tapered small horns, namely small tubes and slits whose cross-sectional area varies monotonically from one end to the other, could be of practical interest. The analytical approach used herein to express the transfer impedance of these small waveguide involves the one dimensional Webster's horn equation which accounts for the thermo-viscous boundary layer effects. An approximate solution which relies on the Volterra integral equation and a 2-D axisymmetrical numerical simulation, using an adaptive mesh, against which the approximate analytical result is tested, show that the analytical approach is appropriate to addressing specific examples, when the length of the horn is much lower than the shortest wavelength of interest, the radius (or thickness) of the horn being of the same order of magnitude as the boundary layer thicknesses.

**PACS no. 43.20.Mv, 43.20.Hq, 43.90.+v**

## 1. Introduction

Being concerned by the use of small tubes and slits filled with thermo-viscous fluid for obtaining specific properties when designing small scale acoustic devices, slowly tapered small horns, namely small tubes and slits whose cross-sectional area varies monotonically from one end to the other, could be of practical interest. Although the class of devices which are made up of these small tapered tubes or slits is limited, it could be sufficiently broad to be of interest because it could be helpful to those designing very small (even miniaturized) components (displayed examples are for small transducers, earplugs, and others).

Besides accounting for the geometrical effects of varying cross-sectional area, the formulation used herein gives a prominent role to the viscous and thermal boundary layers because both their thicknesses have the same order of magnitude as the cross-sectional dimensions of the horn and their effects depend on the axial coordinate of the horn.

The approach involves the one dimensional Webster's horn equation [1, 2, 3, 4, 5] which accounts for the boundary layer effects [4, 6, 7, 8, 9, 10, 11]. An approximate representation which involves successively a change of variables, the Volterra integral equation, and iterative process belong Born approximation to seek the solutions is established for the transfer impedance of these small waveguides. This representation enables analytical estimates to be found in the "long wavelength range" (when the transverse dimensions of the horn are much lower than the shortest wavelength $\lambda_S$ of interest and the length of the horn is lower than $\lambda_S$). In previous studies, several authors [8, 12, 13] consider solutions formed by products of matrices (the horn being considered as a succession of finite elements) or a step by step numerical solutions of second order equations. Compared to these approaches, the benefit of the formal solution outlined below (Volterra equation) comes from the fact that we consider only one global transfer matrix. Nevertheless it has in fact a marked shortcoming in term of computational convenience because it implies that one should first calculate the integrals in each element of the transfer matrix, but these integrals are very simple to handle. Numerical solutions [14, 15, 16] relying on a specific finite element program, against which the approximate analytical results are tested, are given, showing moreover particle velocity fields, temperature variation fields and pressure fields.

The formulation is appropriate to addressing specific examples, namely both tapered cylindrical tubes and tapered rectangular slits, the shape of which being, among others, conical, exponential or power of the axial variable (Bessel's horn) and the radius (or thickness) of which being of the same order of magnitude as the boundary layer thicknesses. The results may be helpful to those seeking benchmark solutions and analytic insight.

The procedural aspects are described in sections 2 and 3, along with the resultant formula, while supplementary details in a particular case (exponential horn) and further approximation are relegated to the appendices A to C. The

Received 11 April 2013,
accepted 1 July 2013.

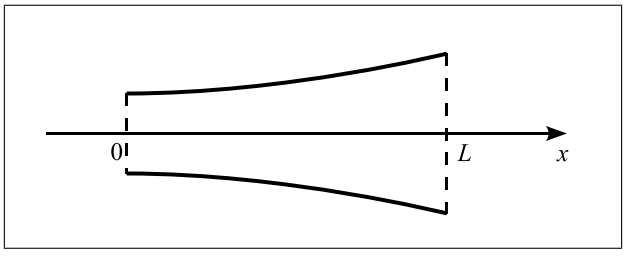


Figure 1. The tapered element (tube or slit). Depending on the section or figure considered below, $x = 0$ is the entrance or the end (the contrary for $x = L$).

2-D axysimmmetrical numerical simulation is outlined in section 4. Then, results obtained from both analytical approach and numerical implementation are presented and discussed in section 5 and 6.

## 2. Basic equations

Owing to the fact that the rigid-walled horn of finite length is slowly tapered, the only coordinate involved in the approach used for describing the pressure variation is the axial coordinate of the horn (denoted $x$). The pressure variation is assumed to be constant through the cross-sectional areas. The origin $x = 0$ is set at the left end (Figure 1), the coordinate of the other end being denoted $L$. In the interval $x \in (0, L)$, the cross-sectional dimension, *i.e.* the radius (cylindrical) or the thickness (slit), has the same order of magnitude as the thickness of the viscous and thermal boundary layers.

The appropriate basic equations are those given primarily by Zwikker and Kosten [6], which lead to, for tapered horns [8],

$$\partial_x p(x) = -\frac{Z_v(x)}{S(x)} U(x), \tag{1a}$$

$$\partial_x U(x) = -Y_t(x)\, S(x)\, p(x), \tag{1b}$$

where $p(x)$ and $U(x)$ are respectively the acoustic pressure and the volume velocity in the horn, $S(x)$ denoting the cross-sectional area of the horn and $\partial_x$ standing for $\partial/\partial x$, and where (with a time factor given by $\mathrm{e}^{\mathrm{i}\omega t}$)

$$Z_v(x) = \frac{\mathrm{i}\omega\rho_0}{F_v(x)}, \tag{2a}$$

$$Y_t(x) = \frac{\mathrm{i}\omega}{\rho_0 c_0^2}\left[\gamma - (\gamma-1)F_h(x)\right], \tag{2b}$$

are respectively the series impedance per unit length (related to the viscous boundary layer effects) and the shunt admittance per unit length (related to the thermal boundary layer effects) with [4, 8, 9]

$$F_{h,v}(x) = 1 - \frac{\tan\left[k_{h,v}\epsilon(x)/2\right]}{k_{h,v}\epsilon(x)/2}, \tag{3a}$$

for a slit of thickness $\epsilon(x)$,

$$F_{h,v}(x) = 1 - \frac{2}{k_{h,v}R(x)} \frac{J_1\left[k_{h,v}R(x)\right]}{J_0\left[k_{h,v}R(x)\right]}, \tag{3b}$$

for a tube of radius $R(x)$, $k_v$ and $k_h$ being the wavenumbers associated respectively to the viscous (shear) and thermal diffusion processes given by (when the coordinate normal to the wall is inwardly directed)

$$k_v = \frac{1-\mathrm{i}}{\sqrt{2}}\sqrt{\frac{\rho_0\omega}{\mu}}, \quad k_h = \frac{1-\mathrm{i}}{\sqrt{2}}\sqrt{\frac{\rho_0\omega C_P}{\lambda_h}}. \tag{3c}$$

These complex functions account for the angular frequency $\omega$ of the field and the properties of the fluid, namely the adiabatic compressibility $\chi_0$ and the density $\rho_0$ through the adiabatic speed of sound $c_0$, the heat capacity at constant pressure per unit of mass $C_P$, the specific heat ratio $\gamma$, the shear viscosity coefficient $\mu$, and the thermal conduction coefficient $\lambda_h$.

The appropriate wave equation is the one-dimensional Webster's horn equation which governs the pressure variation, assumed herein to be driven by a uniform acoustic pressure $p(0)$ at the input $x = 0$ of the horn. Using equations (1a, 1b) it is expressed as follows:

$$\left[\partial_{xx}^2 + \sigma(x)\partial_x + k_0^2 f(x)\right] p(x) = 0, \tag{4}$$

where $k_0^2 f(x)$ is the usual appropriate wavenumber (which depends on the x-coordinate) involving the boundary layer effects with

$$k_0 = \frac{\omega}{c_0} \quad \text{(adiabatic wavenumber)},$$

$$f(x) = \frac{\gamma - (\gamma-1)F_h(x)}{F_v(x)}, \tag{5}$$

and where

$$\sigma(x) = \partial_x G(x)/G(x), \tag{6}$$

with $G(x) = F_v(x)S(x)$ (see the particular case of exponential horn in Appendix A1).

Given the following change of variable, which is a particular case of the change of variable used when dealing with Sturm-Liouville equation,

$$x \to \xi = \int_0^x \left[1/G_0(x')\right] \mathrm{d}x', \tag{7a}$$

with $G_0(x) = G(x)/G(0)$, which implies

$$\partial_x \xi = \frac{1}{G_0(x)}, \quad \partial_x p = \frac{1}{G_0(x)}\partial_\xi p, \tag{7b}$$

$$\text{and} \quad \partial_{xx}^2 p = \frac{1}{G_0(x)}\left[\frac{1}{G_0(x)}\partial_{\xi\xi}^2 p - \sigma(x)\partial_\xi p\right], \tag{7c}$$

the first order spatial derivative (equation 4) can readily be removed, and what results is:

$$\left[\partial_{\xi\xi}^2 + k_0^2\phi(\xi)\right] p(\xi) = 0, \tag{8}$$

where

$$\phi(\xi) = G_0^2(x)\, f(x). \tag{9}$$

Note that the same notation $p$ is used for denoting indifferently the pressure variation before $[p(x)]$ and after $[p(\xi)]$ the change of variable. At the input of the horn $\xi(x = 0) = 0$, and at its output the length $\ell$ is defined as $\ell = \xi(x = L)$.

## 3. Analytical solution

Exact analytical solution of such a complex differential equation (8) is unknown to our knowledge, even if the integral which appears in equation (7a) could be expressed easily. Only numerical or approximate analytical solution (which are numerous) can be sought.

The analytical solution of the Helmholtz equation (8) sought herein can be formally expressed from using the following equivalent couple of equations

$$\begin{cases} \partial_\xi q(\xi) + k_0^2\, \phi(\xi)\, p(\xi) = 0, \\ \partial_\xi p(\xi) = q(\xi). \end{cases} \tag{10a}$$

The quantity $q$ may be thought of as proportional to the complex amplitude of the time rate at which volume of fluid is being added to the medium per unit of time through the unit surface, namely the volume velocity field $U(x)$ (equation 1a). By integration over the interval $(0, \xi)$, and integrating the second equation by part, this couple of equation leads readily to the Volterra integral equations (see for example [17]),

$$\begin{cases} \partial_\xi p(\xi) = \partial_\xi p(0) - k_0^2 \displaystyle\int_0^\xi \phi(\zeta)\, p(\zeta)\, \mathrm{d}\zeta, \\ p(\xi) = p(0) + \partial_\xi p(0)\, \xi - k_0^2 \displaystyle\int_0^\xi (\xi - \zeta)\, \phi(\zeta)\, p(\zeta)\, \mathrm{d}\zeta. \end{cases} \tag{10b}$$

The order of magnitude of the last term in the right hand side of this equation is given by the square of the ratio of the length of the horn and the wavelength, *i.e.*

$$\left(\frac{k_0 \ell}{2\pi}\right)^2 = \left(\frac{\ell}{\lambda}\right)^2. \tag{10c}$$

Then, assuming the hypotheses presented above in the introduction, this term is assumed to be much lower than the zero order pressure linear profile (denoted $p_0$),

$$p_0(\xi) = p(0) + \partial_\xi p(0)\, \xi. \tag{11}$$

It follows that the Born approximation of equation (10b) leads to the first order solution

$$\begin{aligned} p_1(\xi) \;&=\; p(0) + \partial_\xi p(0)\, \xi \\ &\quad - k_0^2 \int_0^\xi (\xi - \zeta)\, \phi(\zeta)\, \left[p(0) + \partial_\zeta p(0)\, \zeta\right]\, \mathrm{d}\zeta, \end{aligned} \tag{12}$$

or, using the notation $M_n(\xi) = \int_0^\xi \zeta^n\, \phi(\zeta)\, \mathrm{d}\zeta,\ n = 0, 1, 2,$

$$\begin{aligned} p_1(\xi) \;&=\; p(0)\, \left\{1 - k_0^2\, [\xi M_0(\xi) - M_1(\xi)]\right\} \\ &\quad + \partial_\xi p(0)\, \left\{\xi - k_0^2\, [\xi M_1(\xi) - M_2(\xi)]\right\}. \end{aligned} \tag{13}$$

The particle velocity takes then the following form:

$$\begin{aligned} \partial_\xi p(\xi) \;&=\; \partial_\xi p(0) - k_0^2 \int_0^\xi \phi(\zeta) p(\zeta)\, \mathrm{d}\zeta \\ &\cong\; \partial_\xi p(0) - k_0^2 \int_0^\xi \phi(\zeta)\, \left[p(0) + \partial_\zeta p(0)\, \zeta\right]\, \mathrm{d}\zeta, \end{aligned} \tag{14}$$

namely (Born approximation)

$$\partial_\xi p_1(\xi) = \partial_\xi p(0)\, \left[1 - k_0^2 M_1(\xi)\right] - p(0)\, k_0^2 M_0(\xi). \tag{15}$$

Then, the first order solution ($\ell/\lambda_S < 1$, equation 10c) can be expressed as

$$p_1(\xi) \;=\; A(\xi) p(0) + B(\xi)\, \partial_\xi p(0), \tag{16a}$$

$$\partial_\xi p_1(\xi) \;=\; D(\xi)\, \partial_\xi p(0) - C(\xi) p(0), \tag{16b}$$

with

$$A(\xi) \;=\; 1 - k_0^2\, [\xi M_0(\xi) - M_1(\xi)], \tag{17}$$

$$B(\xi) \;=\; \xi - k_0^2\, [\xi M_1(\xi) - M_2(\xi)], \tag{18}$$

$$C(\xi) \;=\; k_0^2 M_0(\xi), \tag{19}$$

$$D(\xi) \;=\; 1 - k_0^2 M_1(\xi), \tag{20}$$

the successive approximations of higher orders ($p_i$, $i > 1$) being readily obtained from iterating the process (see Appendix A2). Note that the integrals $M_n$ can be easily calculated numerically.

### 3.1. Transfer matrix

Given the volume velocity field $U(\xi)$ (equation 1a)

$$U(\xi) = -\, \{G(0)/(\mathrm{i}\omega\rho_0)\}\, \partial_\xi p(\xi), \tag{21}$$

equations (16a) and (16b) can be written as ($\xi < \lambda_S$)

$$\begin{pmatrix} p(\xi) \\ U(\xi) \end{pmatrix} = \begin{pmatrix} A(\xi) & B(\xi)/h_0 \\ -h_0 C(\xi) & D(\xi) \end{pmatrix} \begin{pmatrix} p(0) \\ U(0) \end{pmatrix}, \tag{22}$$

where $h_0 = -G(0)/(\mathrm{i}\omega\rho_0)$.

### 3.2. Input impedance

The horn is loaded at its end $x = 0$ by the impedance denoted $Z_{out} = p(0)/[-U(0)]$ (here the impedance of a small cylindrical cavity). The impedance at the entrance $x = L$, ($\xi = \ell$) of the horn can be then expressed, from using transfer matrix (22), as

$$Z_{in} = \frac{p(\ell)}{-U(\ell)} = \frac{A(\ell) - B(\ell)/[Z_{out} h_0]}{C(\ell) h_0 + D(\ell)/Z_{out}}. \tag{23}$$

## 4. Numerical solution

Results obtained from numerical implementation can be given for final designs of devices, against which the approximate analytical results can be tested. Such an implementation has been handled herein; it relies on a 2-D axisymmetrical numerical simulation using an adaptive mesh and accounting for the viscous and thermal boundary layer effects [14].

The linear formulation used to perform the numerical modelling is based upon two coupled equations involving the particle velocity $\boldsymbol{v}$ and the temperature variation $\tau$ (the acoustic pressure $p$ being expressed in terms of these two variables) [11]. These two variables are subject to Dirichlet conditions on the rigid isothermal boundaries ($\boldsymbol{v} = \boldsymbol{0}$,

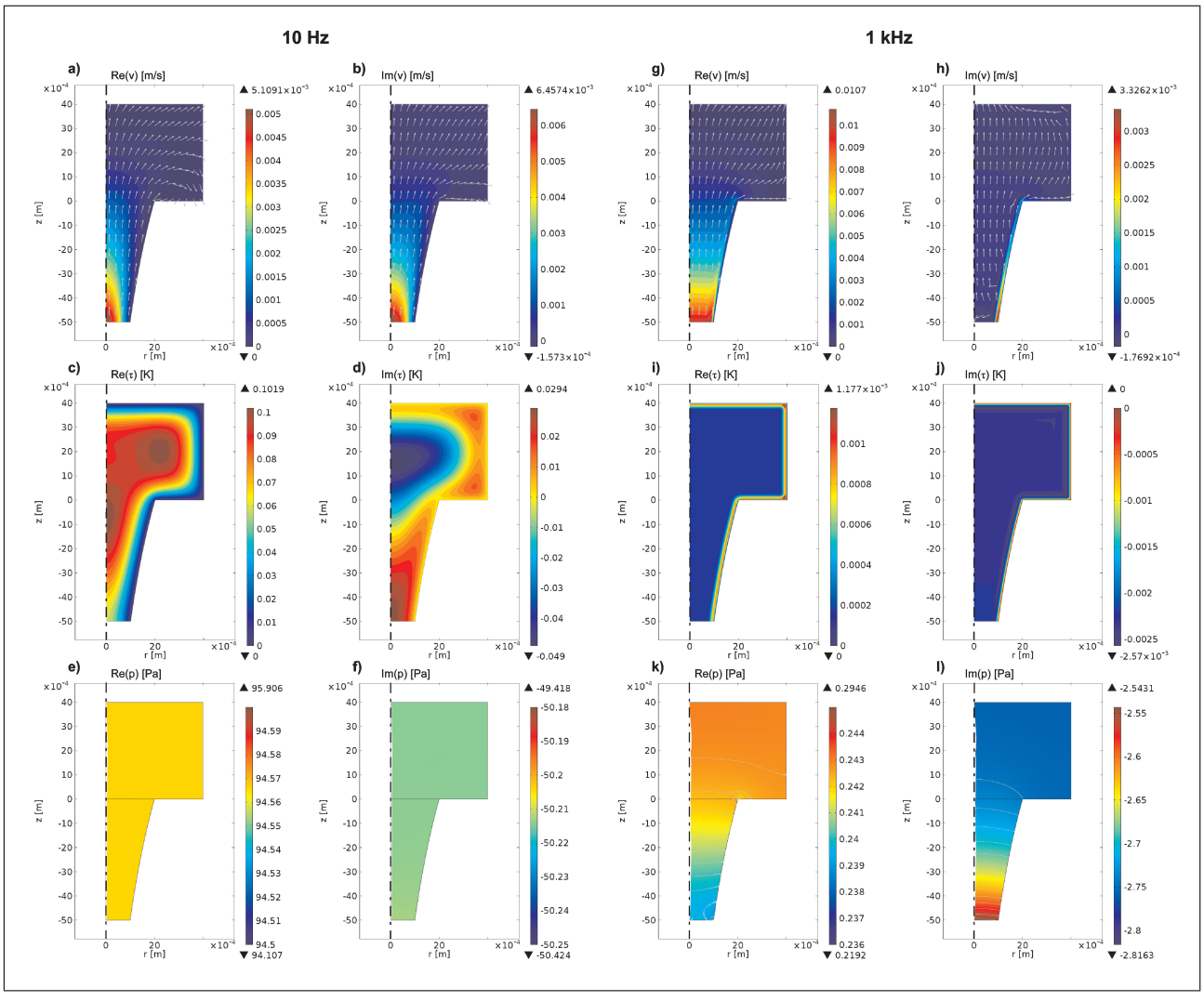


Figure 2. Numerical results for the divergent exponential horn loaded by a small cylindrical cavity: real part - a) at 10 Hz and g) at 1 kHz - and imaginary part - b) at 10 Hz and h) at 1 kHz - of particle velocity field, real part - c) at 10 Hz and i) at 1 kHz - and imaginary part - d) at 10 Hz and j) at 1 kHz - of temperature variation field, and real part - e) at 10 Hz and k) at 1 kHz - and imaginary part - f) at 10 Hz and l) at 1 kHz - of acoustic pressure field (with grey isolines).

$\tau = 0$). A time-periodic source set at the entrance $x = L$ is a virtual adiabatic ($\partial_n \tau = 0$) source described by its normal velocity

$$v_z(r) = v_0 \left[1 - \frac{J_0(k_v r)}{J_0(k_v R_{in})}\right], \qquad (24)$$

which is non-uniformly distributed over the section of the horn: it has the same profile as the analytically calculated particle velocity (which accounts for the viscous boundary layer) in the tube of the radius $R_{in}$ which is the same as the one of the horn entrance. Note that the input velocity of such a profile vanishes at the wall of the horn in order to avoid discontinuities of the particle velocity on the rigid boundaries that must satisfy the non-slip condition [15].

## 5. Results

For each example considered hereafter, the results of numerical investigations are presented first. They depict mappings of particle velocity fields, temperature fields, and acoustic pressure fields. Then, results for the input impedances of small tapered horns, obtained from the analytical expressions presented above, are compared to those obtained numerically in order to validate the analytical approximations and evaluate their accuracy. The examples presented involve both convergent and divergent exponential tapered horns (see Appendix A1), the output end of which is loaded by a small cavity. In each example, the dimensions of the tapered horns are assumed to be such as the analytical approach is valid in the lower frequency range, up to approximately 10 kHz (the geometrical and physical parameters are given in table I). For the numerical solution the amplitude of input velocity $v_0$ (equation 24) is set at 0.01 m/s.

Figure 2 shows the mapping of respectively the particle velocity, the temperature field, and the pressure variations at 10 Hz and 1 kHz, when the tapered small element is loaded at its larger end by a small cylindrical cavity. In Figure 2-i,j the temperature field is uniform everywhere except inside the very thin boundary layers. The acoustic

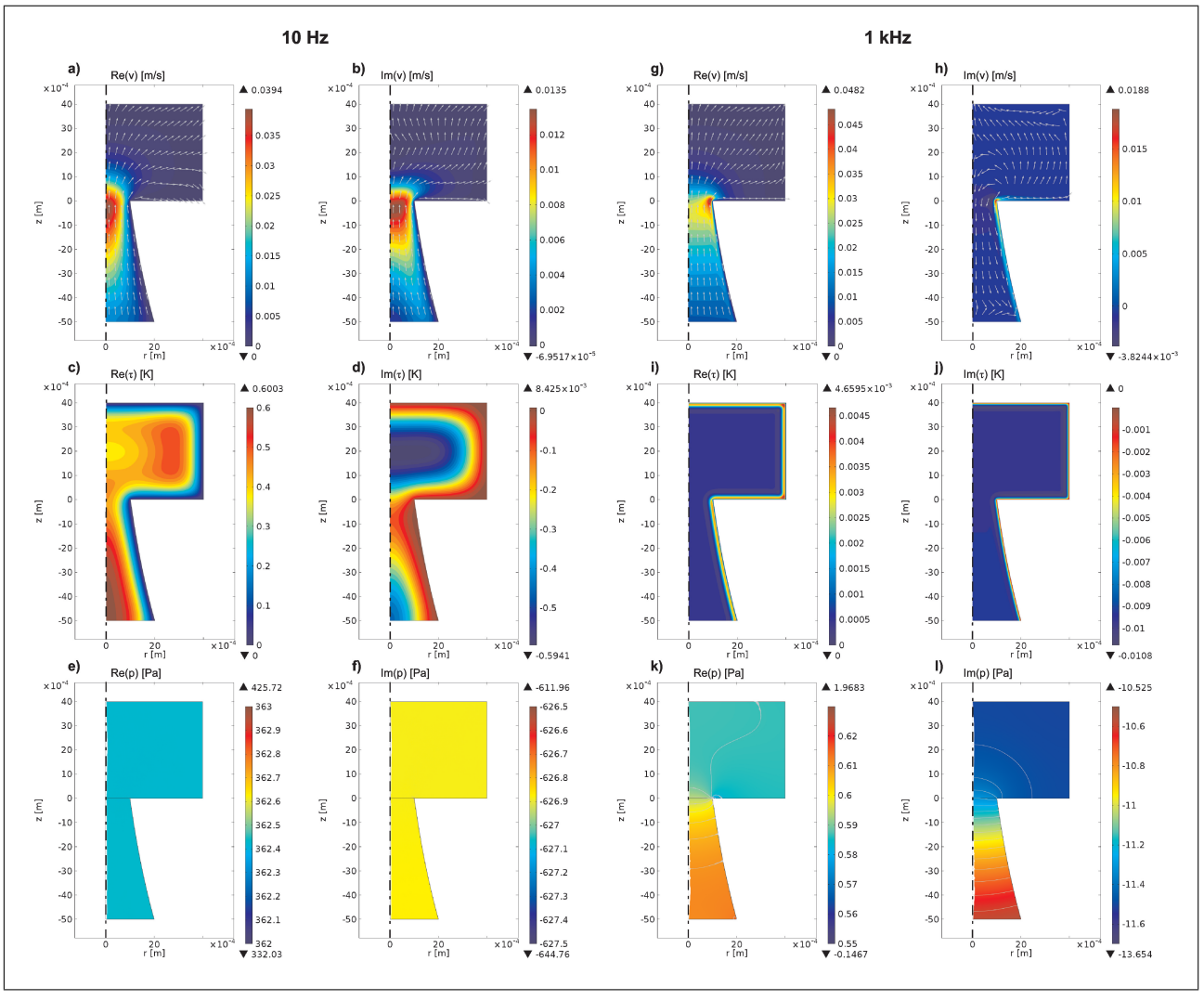


Figure 3. Numerical results for the convergent exponential horn loaded by a small cylindrical cavity: real part - a) at 10 Hz and g) at 1 kHz - and imaginary part - b) at 10 Hz and h) at 1 kHz - of particle velocity field, real part - c) at 10 Hz and i) at 1 kHz - and imaginary part - d) at 10 Hz and j) at 1 kHz - of temperature variation field, and real part - e) at 10 Hz and k) at 1 kHz - and imaginary part - f) at 10 Hz and l) at 1 kHz - of acoustic pressure field (with grey isolines).

pressure field presented in Figure 2-e,f,k,l is quasi-uniform because the dimensions of the cavity are much lower than the wavelength considered.

In Figure 4, the analytically calculated input impedances (amplitudes and phases) of the tapered small element (thick grey solid line) and of cylindrical elements (calculated from using equations (1a) and (1b)) whose the radii are respectively the same as the smaller end one (thin black solid line) and the larger end one (discontinuous grey line) of the tapered element are presented as functions of the frequency, in the frequency range (100 Hz, 30 kHz) and compared with numerical results (black points, 'x' and '+' marks). Analytical results shown in this figure are obtained using the first order Born approximation. It appears clearly both that the Born approximation provides very accurate results in the frequency range of interest (up to 10 kHz for a tapered tube 5 mm long, as expected) and that the behavior of the small tapered element (tube or slit) is approximately the same as an cylindrical element whose the radius (or thickness) would have an intermediate value, between the input one and the output one of the tapered element. Note that Figure 4 involves frequency range (100 Hz, 30 kHz) in order to show clearly the variations of the input impedance in the middle frequency range. In the lower frequency range (10 Hz, 100 Hz) the slope of the curves remains the same as there is for the frequencies just above 100 Hz, as shown below in Figure 6.

The same mappings and results, leading to the same conclusions, are presented in Figures 3 and 5 when the tapered small element is loaded at its smaller end by a small cylindrical cavity. Analytical results for the horn shown in Figure 5 are obtained using the first order Born approximation. Note that the effect of the geometrical discontinuity at the interface between the horn and the cavity is modelled by the usual added mass [7] in the analytical results.

In order to show the ability of the analytical approach to describe the behavior of very thin tapered slits or tubes in frequency range (10 Hz, 10 kHz) such as the radii (or

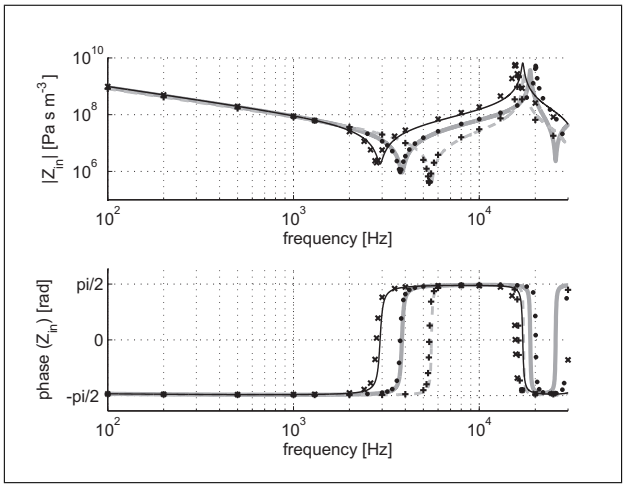


Figure 4. Input acoustic impedance modulus (upper curves) and phase (lower curves) of: i) the divergent exponential horn loaded by a small cylindrical cavity, analytical model (thick grey solid line) and numerical model (black points), ii) the tube of the same radius as the smaller end one of the horn with the same terminal condition as the horn, analytical model (thin black solid line) and numerical model ('x' marks), and iii) the tube of the same diameter as the larger end one of the horn with the same terminal condition as the horn, analytical model (discontinuous grey line) and numerical model ('+' marks).

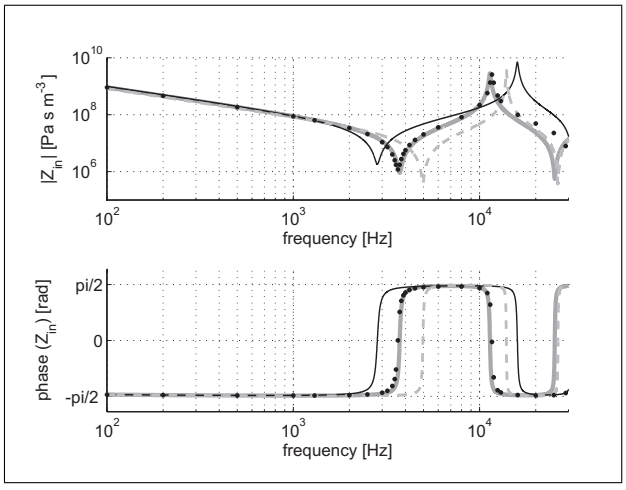


Figure 5. Input acoustic impedance modulus (upper curves) and phase (lower curves) of: i) the convergent exponential horn loaded by a small cylindrical cavity, analytical model (thick grey solid line) and numerical model (black points), ii) the tube of the same radius as the smaller end one of the horn with the same terminal condition as the horn, analytical model (thin black solid line), and iii) the tube of the same diameter as the larger end one of the horn with the same terminal condition as the horn, analytical model (discontinuous grey line).

Table I. Geometrical and physical parameters.

| **Parameter** | **Value** | **Unit** |
|---|---|---|
| Horn length $L$ | $5 \cdot 10^{-3}$ | m |
| Smaller end radius | $1 \cdot 10^{-3}$ | m |
| Larger end radius | $2 \cdot 10^{-3}$ | m |
| Cylindrical cavity height | $4 \cdot 10^{-3}$ | m |
| Cylindrical cavity radius | $4 \cdot 10^{-3}$ | m |
| Static pressure $P_0$ | 101325 | Pa |
| Static temperature $T_0$ | 296.15 | K |
| Density $\rho_0$ | 1.180 | kg/m$^3$ |
| Adiabatic speed of sound $c_0$ | 345.9 | m/s |
| Shear dynamic viscosity $\mu$ | $1.830 \cdot 10^{-5}$ | Pa s |
| Bulk dynamic viscosity $\eta$ | $1.098 \cdot 10^{-5}$ | Pa s |
| Thermal conductivity $\lambda_h$ | $24.40 \cdot 10^{-3}$ | W/m/K |
| Ratio of specific heats $\gamma$ | 1.400 | - |
| Specific heat coefficient at constant pressure per unit of mass $C_P$ | $1.010 \cdot 10^3$ | J/kg/K |

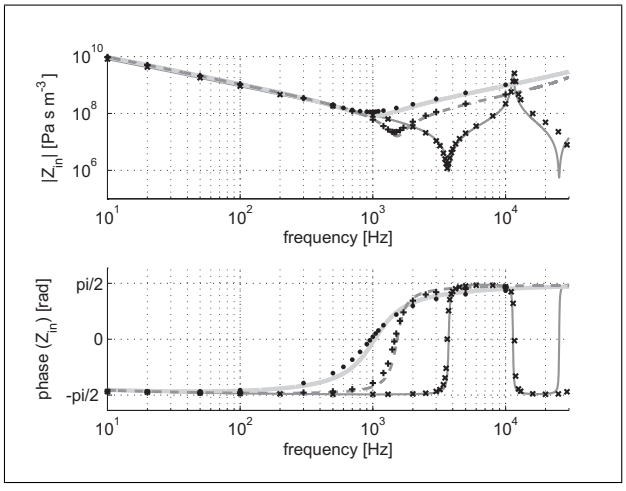


Figure 6. Input acoustic impedance modulus (upper curves) and phase (lower curves) of the convergent exponential horn loaded by a small cylindrical cavity: i) the dimensions of the horn (radius and length) being given in table I - analytical (thin solid grey line) and numerical ('x' marks) model, ii) the dimensions of the horn (radius and length) given in table I divided by 5 - analytical (discontinuous grey line) and numerical ('+' marks) model, and iii) the dimensions of the horn (radius and length) given in table I divided by 10 - analytical (thick solid grey line) and numerical (black points) model.

thicknesses) of these horns can be smaller than the thicknesses of the viscous and thermal boundary layers, Figure 6 shows the modulus (upper curves) and the phase (lower curves) obtained from the analytical first order Born approximation (grey lines) and the numerical simulations (black points, 'x' and '+' marks) for three different tapered horns (and the same cavity as above): the convergent horn considered above (Figure 5) and both the horn whose dimensions are divided by 5 and the one whose dimensions are divided by 10. As expected, the agreement between analytical and numerical results shows that the first order Born approximation permits an analytical characterisation of such components with a good accuracy in the frequency range of interest. There is no low frequency limit of the method (except for the approximation described in Appendix A3). In the high frequency range the limitation of the method appears at frequencies for which the length of the horn is near $\lambda/4$.

## 6. Conclusion

As expected, concerning the transfer impedance of the small horn, these results show clearly that the analytic estimation appears to be well validated by numerical evaluation in the frequency range of interest (up to 10 kHz for the dimensions of the horn given in table I), even when limiting this estimation to the Born approximation in the Voltera integral or the direct lower order approximation. Slight discrepancies remain which could be explained more particularly by numerical uncertainties and analytical approximations.

It results of sufficient accuracy as to serve as exact solution for practical applications. The main feature is that the behavior of the small tapered element (tube or slit) is approximately the same as an element whose the radius (or thickness) would have an intermediate value, between the input one and of the output one of the tapered element. Therefore, the interest of such small horns relies particularly on their ability to have the narrower end which can be inserted in a narrow element while having the properties of a larger component (tube or slit).

## Appendix

### A1. Exponential axisymmetrical horn

When considering the example of exponential axisymmetrical horn, expressions presented in the paper takes the forms presented hereafter. The expressions of the radius is given by

$$R(x) = R(0)\mathrm{e}^{(\alpha/2)x}, \tag{A1}$$

where the parameter $\alpha$ can then be written as

$$\alpha = \frac{1}{L}\ln\left[R^2(L)/R^2(0)\right]. \tag{A2}$$

The change of variable leads respectively to

$$\begin{aligned} \xi &= \int_0^x \frac{F_v(0)R^2(0)}{F_v(x')R^2(x')}\mathrm{d}x', \\ \partial_x\xi &= \frac{F_v(0)R^2(0)}{F_v(x)R^2(x)}, \\ \xi(0) &= 0 \text{ and } \ell = \xi(L). \end{aligned} \tag{A3}$$

The integral $M_n(\ell)$ (13) is then calculated numerically as

$$\begin{aligned} M_n(\ell) &= M_n\big(\xi(x=L)\big) \\ &= \int_0^L \left[\int_0^x \frac{F_v(0)R^2(0)}{F_v(x')R^2(x')}\mathrm{d}x'\right]^n \\ &\quad \cdot \frac{[\gamma-(\gamma-1)F_h(x)]\,R^2(x)}{F_v(0)R^2(0)}\mathrm{d}x. \end{aligned} \tag{A4}$$

The derivative of the function $\phi(\xi)$ in the lower order approximation (A9) can be expressed as

$$\begin{aligned} \partial_\xi\phi(\xi) &= \partial_x\phi(\xi(x))/\partial_x\xi \\ &= \partial_x\left[G_0^2(x)f(x)\right]\frac{F_v(x)R^2(x)}{F_v(0)R^2(0)}. \end{aligned} \tag{A5}$$

### A2. Second order Born approximation and lower order approximation

Introducing the notation

$$P_{p,q}(\xi) = \int_0^\xi \zeta^p\,\phi(\zeta)\,M_q(\zeta)\,\mathrm{d}\zeta, \quad p,q = 0,1,2, \tag{A6}$$

the matrix elements defined in equations (16a, 16b) take the form

$$\begin{aligned} A(\xi) &= 1 - k_0^2\left\{\xi\left[M_0(\xi) + k_0^2\left(P_{0,1}(\xi) - P_{1,0}(\xi)\right)\right]\right. \\ &\quad \left. - M_1(\xi) + k_0^2\left(P_{2,0}(\xi) - P_{1,1}(\xi)\right)\right\}, \\ B(\xi) &= \xi - k_0^2\left\{\xi\left[M_1(\xi) + k_0^2\left(P_{0,2}(\xi) - P_{1,1}(\xi)\right)\right]\right. \\ &\quad \left. - M_2(\xi) + k_0^2\left(P_{2,1}(\xi) - P_{1,2}(\xi)\right)\right\}, \\ C(\xi) &= k_0^2\left\{M_0(\xi) + k_0^2\left[P_{0,1}(\xi) - P_{1,0}(\xi)\right]\right\}, \\ D(\xi) &= 1 - k_0^2\left\{M_1(\xi) + k_0^2\left[P_{0,2}(\xi) - P_{1,1}(\xi)\right]\right\}. \end{aligned} \tag{A7}$$

Note that the integrals $M_n$ and $P_{p,q}$ can be easily calculated numerically.

It is worth noting that a lower order approximation can alternatively result with the help of the following approximation $\partial_\xi f(\xi) \approx [f(\xi) - f(0)]/\xi$, the function $f(\xi)$ representing indifferently $p(\xi)$ or $q(\xi)$. Then, starting from equations (10a), this lower order solution can be expressed as

$$p(\xi) = \frac{p(0) + \xi\,\partial_\xi p(0)}{1 + \xi^2 k_0^2\,\phi(\xi)}. \tag{A8}$$

It follows after some algebra that the matrix elements defined above are approximately given here by

$$\begin{aligned} A(\xi) &\approx \frac{1}{1+\xi^2k_0^2\,\phi(\xi)}, \\ B(\xi) &\approx \frac{\xi}{1+\xi^2k_0^2\,\phi(\xi)}, \\ C(\xi) &\approx \frac{2\xi k_0^2\,\phi(\xi) + \xi^2k_0^2\,\partial_\xi\phi(\xi)}{\left[1+\xi^2k_0^2\,\phi(\xi)\right]^2}, \\ D(\xi) &\approx \frac{1}{1+\xi^2k_0^2\,\phi(\xi)} - \frac{2\xi^2k_0^2\,\phi(\xi) + \xi^3k_0^2\,\partial_\xi\phi(\xi)}{\left[1+\xi^2k_0^2\,\phi(\xi)\right]^2}. \end{aligned} \tag{A9}$$

Note that, to the zeroth-order approximation, which correspond to the limit $G_0(x) = 1$ and $\ell = L$, the well-known result

$$\frac{p(L) - p(0)}{U} \cong \frac{\mathrm{i}\omega\rho_0}{S(0)F_v(0)}L, \tag{A10}$$

for small tubes or slits whose cross-sectional areas do not depend on the axial coordinate, is recovered.

The effect of the second order Born approximation of equation (10b) and the effect of the lower order approximation (A8) are shown in Figure A1. In the frequency range of interest (up to 10 kHz approximately) the second order Born approximation (solid grey line) does not differ significantly from the first order one (discontinuous

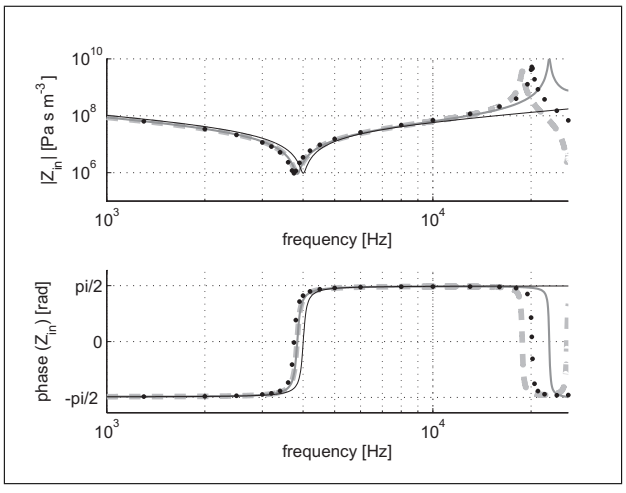


Figure A1. Input acoustic impedance modulus (upper curves) and phase (lower curves) of the divergent exponential horn loaded by a small cylindrical cavity calculated analytically using $1^{st}$ order Born approximation (discontinuous grey line), using $2^{nd}$ order Born approximation (solid grey line), lower order approximation (thin black line) and calculated numerically (black points).

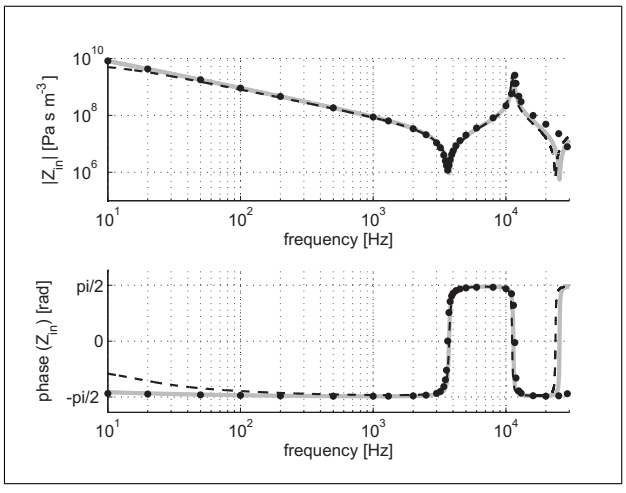


Figure A2. Input acoustic impedance modulus (upper curves) and phase (lower curves) of the convergent exponential horn loaded by a small cylindrical cavity calculated: i) analytically neglecting the variation of the series impedance per unit length $Z_v(x)$ as described in the Appendix C (black dashed line), ii) analytically using the complete model (solid grey line), and iii) numerically (black points).

grey line) while in the higher frequency range the first order Born approximation matchs better with numerical results (black points). The lower order approximation (A8) (thin black line) differs more from the numerical solution than the solution using the Born approximation even below 10 kHz, but remains interesting when looking for the reasonable approximation without using the numerical integration.

### A3. Neglecting the variation of the series impedance per unit length $Z_v(x)$

The approximate solution obtained when neglecting the variation of the series impedance per unit length $Z_v(x)$ in equation (4), leading to replace $G_0(x)$ by $S_0(x) = S(x)/S(0)$ then to write $\sigma(x) = \partial_x S(x)/S(x)$, can be considered in a broad class of situations because it operates usualy in the frequency range of interest (its effect occurs only in the lower frequency range as shown below). Figure A2 shows that this approximation is not suitable only in the lower frequency range (here up to 100 Hz for the convergent tapered horn given in table I), because the discrepancies which appears between the modulus and the phase calculated when assuming this approximation (dashed line) and the ones calculated with the complete analytical model (solid line) (matching well with the numerically calculated results (black points)) are not negligible. The boundary layer thicknesses have the same order of magnitude as the radius of the tube in this lower frequency range, then the iterative impedance $Z_v(x)$ cannot be assumed to be independent of the viscous boundary layer effects.

## References

[1] V. Salmon: Generalized plane wave horn theory. J. Acoust. Soc. Am. **17** (1946) 199–211.

[2] Z. Škvor: Vibrating systems and their equivalent circuits. Elsevier, Amsterdam, 1991.

[3] P. Lesniewski: Discrete component equivalent circuit for Webster's horns. Applied Acoustics **44** (1995) 117–124.

[4] M. Bruneau, T. Scelo: (translator and contributor) Fundamentals of acoustics. ISTE, UK, USA, 2006.

[5] P. Eveno, J.-P. Dalmont, R. Caussé, J. Gilbert: Wave propagation and radiation in a horn: Comparisons between models and measurements. Acta Acustica united with Acustica **98** (2012) 158–165.

[6] C. Zwikker, C. W. Kosten: Sound absorbing materials. Elsevier, Amsterdam, 1949.

[7] A. Chaigne, J. Kergomard: Acoustique des instruments de musique. Belin, Paris, 2008.

[8] R. Caussé, J. Kergomard, X. Lurton: Input impedance of brass musical instruments – Comparison between experiment and numerical models. J. Acoust. Soc. Am. **75** (1984) 241–254.

[9] D. Rodrigues, C. Guianvarc'h, J.-N. Durocher, M. Bruneau, A.-M. Bruneau: A method to measure and interpret input impedance of small acoustic components. Journal of Sound and Vibrations **315** (2008) 890–910.

[10] D. H. Keefe: Acoustical wave propagation in cylindrical ducts: Transmission line parameter approximations for isothermal and nonisothermal boundary conditions. J. Acoust. Soc. Am. **75** (1984) 58–62.

[11] N. Joly, M. Bruneau, R. Bossart: Coupled equations for particle velocity and temperature variation as the fundamental formulation of linear acoustics in thermo-viscous fluids at rest. Acta Acustica united with Acustica **92** (2006) 202–209.

[12] E. V. Jansson, A. H. Benade: On plane and spherical waves in horns with nonuniform flare II. Acustica **31** (1974) 185–202.

[13] G. R. Plitnik, W. J. Strong: Numerical methods for calculating input impedance of the oboe. J. Acoust. Soc. Am. **65** (1979) 816–825.

[14] N. Joly: Finite element modeling of thermoviscous acoustics on adapted anisotropic meshes: Implementation of the particle velocity and temperature variation. Acta Acustica united with Acustica **96** (2010) 102–114.

[15] P. Honzík, N. Joly, S. Durand, D. Rodrigues, J.-N. Durocher, B. M.: Finite element modelling of acoustic field inside small components: Application to an annular slit terminated by an aperture in an infinite screen. Metrologia **49** (2012) 32–40.

[16] R. Barbieri, N. Barbieri: Acoustic horns optimization using finite elements and genetic algorithm. Applied Acoustics **74** (2013) 356–363.

[17] K. Rektorys: Survey of applicable mathematics. Iliffe Books Ltd., London, 1969. in co-edition with SNTL - Publisher of Technical Literature, Prague, section 19.6.